





Optimization of adiabatic frequency conversion in an all-pass resonator

Luis Cortes-Herrera ,* Xiaotong He , Jaime Cardenas , and Govind P. Agrawal 

The Institute of Optics, University of Rochester, Rochester, New York 14627, USA



(Received 2 June 2022; accepted 29 July 2022; published 18 August 2022)

Adiabatic frequency conversion (AFC) is a promising alternative for shifting the frequency of optical signals. In this paper we present a comprehensive theoretical study of the energy efficiency of AFC in an all-pass resonator. Through the Cauchy-Schwarz inequality, we deduce the upper limit of the energy efficiency of the AFC process and analyze its dependence on the input pulse shape. For a fixed pulse shape, we discuss the dependence of the AFC efficiency on its relevant timescales. We show that maximum efficiency requires overcoupling of the resonator to a degree dependent on the input pulse duration. We compare and contrast the requirements for optimal AFC for pulsed and continuous-wave inputs.

DOI: [10.1103/PhysRevA.106.023517](https://doi.org/10.1103/PhysRevA.106.023517)

I. INTRODUCTION

In photonics, frequency conversion is usually realized via nonlinear wave mixing. In particular, the advent of integrated photonics has enabled broadband and efficient wave mixing on a chip with a compact footprint [1–4]. Despite its successes, integrated wave mixing has inherent limitations [5–7]. First, it demands a high-power optical pump, which impedes on-chip integration. Second, wave mixing must obey the conservation of photon energy. Consequently, to tune the output signal’s frequency, one must change the frequency of either the input signal or the pump. Third, efficient wave mixing requires phase matching. This requirement restricts both the waveguide geometry and the range of possible output frequencies.

Adiabatic frequency conversion (AFC) is a promising alternative for frequency shifting. Adiabatic frequency conversion is the phenomenon in which light excites an optical cavity’s mode, the cavity’s refractive index is modulated, and light follows the cavity’s instantaneous resonance frequency [8,9]. This process is called adiabatic because it was shown numerically [9] that it preserves the adiabatic invariant of a harmonic oscillator [10,11]. In contrast to wave mixing, AFC does not require optical pumping or phase matching and is not restricted by photon-energy conservation. Furthermore, its output frequency can be tuned by adjusting the strength of the index modulation within the cavity. Therefore, AFC can be used to realize tunable frequency conversion in a photonic chip. Adiabatic frequency conversion has been demonstrated in silicon cavities [12–16] and semiconductor-based metasurfaces [17] through charge-carrier injection, in a silica toroidal cavity through the optical Kerr effect [18], and in a bulk lithium niobate resonator [19] through the Pockels effect.

So far, theoretical work on AFC has focused either on its modeling and description [8,9,20–22] or on its proposal for novel applications [8,23–25]. Discussion of the AFC efficiency has attracted less attention. It was found in Ref. [26]

that AFC in an all-pass (i.e., Gires-Tournois) resonator can yield an energy efficiency of 74%. However, a comprehensive theoretical study of AFC efficiency, which analyzes all its limitations and determines the conditions for optimal efficiency, is still lacking. That is the objective of our work. We hope that our study will help move the investigation of AFC from proof-of-principle demonstrations to engineering practical devices for diverse applications.

Adiabatic frequency conversion has been analyzed through two semianalytic approaches. One approach is based on heuristic traveling-wave models [20,21,27]. In these, an intuitive ansatz is proposed for optical wave propagation in a dynamic medium, inferred from generalizing wave propagation in static cavities. Although this approach is intuitive by construction, it is unclear how to derive their ansatz from Maxwell’s equations. As a result, its accuracy cannot be judged without comparing directly with experiments or an independent analysis.

The other approach employs the time-domain coupled-mode equations that describe the time evolution of a discrete set of resonator modes [22,23,25,26,28]. The main advantage of this approach is the simplicity of the resulting equations, which reduce the electromagnetic field to a finite number of degrees of freedom. Moreover, this approach can be derived directly from Maxwell’s equations [22,28]. Hence, conditions sufficient for its validity can be obtained, and its accuracy can be assessed *a priori*. For these reasons, we analyze AFC in this paper using the coupled-mode approach.

The remainder of the paper is organized as follows. In Sec. II we describe the system under analysis, write the governing coupled-mode equations, and find a general expression for the AFC energy efficiency in the high-modulation limit. In Sec. III we use the Cauchy-Schwarz inequality to examine the theoretical limit of energy efficiency for AFC and to analyze the dependence of energy efficiency on input pulse shape. We also explain how the ideal input pulse shape to excite AFC emerges directly from energy conservation and reversibility in time. In Sec. IV we consider a fixed single-lobe input pulse shape and analyze how the energy efficiency of AFC varies as we change the various timescales of the process. We

*lcortesh@ur.rochester.edu

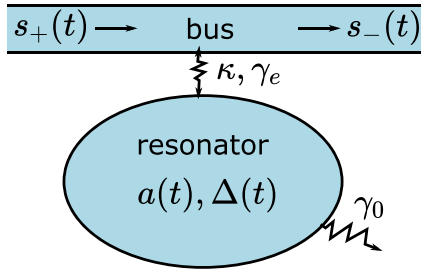


FIG. 1. Schematic the bus-resonator system used for adiabatic frequency conversion.

obtain simple formulas to maximize the energy efficiency of AFC for any given pulse duration. In Sec. V we consider a continuous-wave input of fixed power and analyze the energy of the resulting AFC output. We compare the results with those of Sec. IV and explain the similarities and differences. In Sec. VI we summarize and present the paper's conclusions.

II. ANALYSIS OF GOVERNING EQUATIONS

We consider the configuration depicted in Fig. 1. It consists of an optical all-pass resonator (i.e., a resonating structure with a single input port and a single output port [26,29,30]) under temporal modulation of its refractive index. Typical examples of all-pass resonators are a Gires-Tournois étalon, a microring resonator directionally coupled to a waveguide, and a photonic-crystal cavity butt coupled to a photonic crystal waveguide. An optical pulse is injected into the input port with a carrier frequency ω equal to that of a specific resonance ω_c of the resonator before modulation. As a result, a large fraction of the input pulse's energy is coupled into the resonator. The amplitude a of the excited resonator mode is normalized so that $|a|^2$ represents the mode's energy before modulation. Modulation of the resonator changes the refractive index, which in turn changes the mode's instantaneous frequency $\omega_c(t)$. The evolution of the mode's amplitude is governed by the well-known differential equation [23–25]

$$\frac{da}{dt} = -i\Delta(t)a - \gamma a + \kappa s_+(t). \quad (1)$$

Here $\Delta(t) = \omega_c(t) - \omega$ is the detuning from the resonance; $s_+(t)$ is the input amplitude, normalized such that $|s_+(t)|^2$ is its instantaneous power; κ is a coupling coefficient; and γ is the mode's decay rate, inversely proportional to the cavity's Q parameter. In general, γ consists of two contributions: an intrinsic decay rate γ_0 , independent of output coupling, and the extrinsic decay rate γ_e , resulting from coupling of the resonator to the output port [31,32]. Thus we have the relation

$$\gamma = \gamma_0 + \gamma_e. \quad (2)$$

In an AFC experiment, the cavity's resonance frequency is modulated monotonically. For simplicity, we assume that the modulation occurs in a steplike fashion over a timescale shorter than the half photon lifetime γ^{-1} and the duration of $s_+(t)$. In this case, $\Delta(t)$ can be modeled as

$$\Delta(t) = \Delta_0 H(t - t_0). \quad (3)$$

Here t_0 is the time at which modulation starts, $H(t)$ the Heaviside function, and Δ_0 the postmodulation detuning of the cavity with respect to its original resonance.

To complete the description of AFC in an all-pass resonator, we must also consider the output wave $s_-(t)$ leaving the resonator. It is given by [32]

$$s_-(t) = \exp(i\phi) s_+(t) + \kappa a(t), \quad (4)$$

where ϕ is a constant phase that depends on the planes where $s_+(t)$ and $s_-(t)$ are defined. From energy conservation and time-reversibility considerations, it can be shown that κ in Eq. (1) and κ in Eq. (4) must indeed be identical [31]. Increasing the coupling between the resonator and the bus increases both κ and γ_e . Hence, it is critical to model the relation between these two parameters to model and optimize AFC. This is accomplished via energy-conservation arguments and results in the relation [31]

$$\kappa = \sqrt{2\gamma_e}. \quad (5)$$

After the cavity undergoes modulation, we expect two things to happen. First, we expect the light contained therein to follow the new frequency. Second, we expect the coupling of the input $s_+(t)$, oscillating at the original resonance frequency, into the mode amplitude $a(t)$ to become inefficient. To verify these two expectations, it is convenient to introduce a change of variable for $t > t_0$, from the rapidly oscillating $a(t)$ to the slowly oscillating $\tilde{a}(t)$, defined through

$$a(t) = \tilde{a}(t) \exp[-(i\Delta_0 + \gamma)(t - t_0)]. \quad (6)$$

Substituting Eq. (6) into Eq. (1) and integrating the resulting differential equation, we obtain

$$\tilde{a}(t) = a(t_0) + \int_{t_0}^t dt' \kappa s_+(t') \exp[(i\Delta_0 + \gamma)(t' - t_0)]. \quad (7)$$

If the second term on the right-hand side of Eq. (7) can be neglected, then both of our expectations would be correct. In that case, $\tilde{a}(t)$ would be a constant and $a(t)$ would oscillate at the frequency Δ_0 , as indicated in Eq. (6). Also, $s_+(t)$ would have no effect, as it would not couple appreciably to $a(t)$. In the Appendix we show that neglect of the integral in Eq. (7) is justified if

$$8\gamma_e \ll T_s \Delta_0^2, \quad (8)$$

where T_s is the duration of the input pulse $s_+(t)$.

When Eq. (8) holds, Eq. (6) shows that $a(t)$ oscillates at the frequency Δ_0 and decays exponentially for $t > t_0$. Given the output relation in Eq. (4), $s_-(t)$ will lead to interference between $a(t)$ and the input $s_+(t)$ at the original frequency. Let us assume the original frequency is filtered out from $s_-(t)$. Then the output energy U_c at the converted frequency is a function of the modulation time t_0 and can be evaluated as

$$U_c = \int_{t_0}^{\infty} dt |s_-(t)|^2 = \frac{\gamma_e}{\gamma} |a(t_0)|^2. \quad (9)$$

Thus, we can maximize U_c if we maximize the product $(\gamma_e/\gamma)|a(t_0)|^2$. Because Eq. (1) is linear in $a(t)$, it proves

convenient to consider the auxiliary variable

$$a_c(t_0) = \sqrt{\frac{\gamma_e}{\gamma}} a(t_0). \quad (10)$$

As $U_c = |a_c(t_0)|^2$, the output energy $U_c(t_0)$ is maximum whenever $|a_c(t_0)|$ is. Therefore, $a_c(t_0)$ can be interpreted as a converted-energy amplitude, just as $a(t)$ is the instantaneous energy amplitude of the resonator mode. We rewrite Eq. (1) as a differential equation for $a_c(t_0)$ and obtain

$$\frac{da_c}{dt_0} = -\gamma a_c + \sqrt{\frac{2\gamma_e^2}{\gamma}} s_+(t_0). \quad (11)$$

Equation (11) is the main result of this section and its solutions are the subject of interest in the following sections. We emphasize that the modulation time t_0 is the independent variable in this equation.

III. UPPER LIMIT ON ENERGY EFFICIENCY

Usually, the cavity undergoing AFC is unexcited before the incident pulse $s_+(t)$ starts driving it. Let T be the time during which the input pulse $s_+(t)$ couples with the cavity before AFC is induced. By this definition, cavity excitation starts at $t_0 - T$. Then $a_c(t) = 0$ for $t \leq (t_0 - T)$ and Eq. (11) can be integrated to yield

$$a_c(t_0) = \int_{-\infty}^{\infty} dt h(t_0, t) s_+(t), \quad (12)$$

where $h(t_0, t)$ is the impulse response of Eq. (11) and is given by

$$h(t_0, t) = \sqrt{\frac{2\gamma_e^2}{\gamma}} \exp[-\gamma(t_0 - t)] \times [H(t + T - t_0) - H(t - t_0)]. \quad (13)$$

Recalling that the input $s_+(t)$ is normalized so that $|s_+(t)|^2$ is its instantaneous power, the input's total energy U_s is evaluated as

$$\int_{-\infty}^{\infty} dt |s_+(t)|^2 = U_s. \quad (14)$$

We are interested in maximizing the converted energy U_c , i.e., the square modulus of $a_c(t_0)$. To do so, we make two observations. First, Eq. (12) suggests that $a_c(t_0)$ can be interpreted as an inner product of two complex-valued functions: $h^*(t_0, t)$ and $s_+(t)$. Second, it follows from Eqs. (13) and (14) that both $h^*(t_0, t)$ and $s_+(t)$ are square integrable. From these two facts we conclude that U_c is bounded from above by the Cauchy-Schwarz (CS) inequality for square-integrable functions [33]

$$\left| \int_{-\infty}^{\infty} dt h(t_0, t) s_+(t) \right|^2 \leq \int_{-\infty}^{\infty} dt |h(t_0, t)|^2 \int_{-\infty}^{\infty} dt |s_+(t)|^2. \quad (15)$$

From Eq. (14), the second integral on the right-hand side of Eq. (15) evaluates to U_s . On the other hand, the first integral can be evaluated by substituting Eq. (13) for $h(t_0, t)$. In this

manner, we readily obtain

$$\int_{-\infty}^{\infty} dt |h(t_0, t)|^2 = \left(\frac{\gamma_e}{\gamma} \right)^2 [1 - \exp(-2\gamma T)]. \quad (16)$$

In evaluating Eq. (16), we made use of Eq. (5), relating κ and γ_e .

Then substituting Eqs. (14) and (16) into the right-hand side of Eq. (15) and recalling that the left-hand side of Eq. (15) equals the converted energy U_c , we obtain the bound

$$U_c \leq U_s \left(\frac{\gamma_e}{\gamma} \right)^2 [1 - \exp(-2\gamma T)]. \quad (17)$$

Equation (17) is an important result showing the upper bound on the maximum energy efficiency, $\eta = U_c/U_s$, for AFC in an all-pass resonator. Because both factors $(\gamma_e/\gamma)^2$ and $1 - \exp(-2\gamma T)$ are bounded by unity, Eq. (17) is stricter than the intuitively evident condition that the output energy cannot exceed the input energy, i.e., $U_c \leq U_s$. Equation (17) is imposed solely by the resonator and the modulation scheme, specifically, by the ratio of extrinsic to intrinsic decay rate and the time T between the start of the pulse $s_+(t)$ and the start of the index modulation.

Even for an ideally shaped pulse (discussed below) and modulation satisfying $\gamma T \gg 1$, Eq. (17) restricts the energy efficiency η by $(\gamma_e/\gamma)^2$ rather than the intuitive limit of $\eta \leq 1$. Still, this additional factor of $(\gamma_e/\gamma)^2$ makes intuitive sense. One factor of γ_e/γ arises from Eq. (10). It reflects the fact that not all the energy in the cavity at time of modulation exits into the bus, but only a fraction of γ_e/γ . The second factor of γ_e/γ accounts for the fact that intrinsic loss γ_0 causes coupling to be imperfect. Even for an ideally shaped pulse, only a fraction γ_e/γ of the incident pulse's energy can be coupled into the resonator because energy continuously dissipates into the environment.

The bound in Eq. (17) increases with γT , where T is the delay between the start of the pulse and the start of index modulation. However, increasing γT for a fixed pulse shape does not always increase efficiency of AFC. Such an increase in energy efficiency only needs to hold for the ideal pulse shape, for which the CS inequality becomes an equality.

A well-known corollary of the CS inequality (15) is that it becomes an equality if and only if the two functions in the inner product, $s_+(t)$ and $h^*(t_0, t)$, are linearly dependent [33]. It follows from Eq. (13) that this can occur if and only if the input $s_+(t)$ has the form

$$s_+(t) = \sqrt{2\gamma U_s} [1 - \exp(-2\gamma T)]^{-1/2} \exp[-\gamma(t_0 - t)] \times [H(t + T - t_0) - H(t - t_0)], \quad (18)$$

where $s_+(t)$ has been normalized according to Eq. (14). This relation shows that, to achieve the maximum η allowed by Eq. (17), $s_+(t)$ must start at the time $t_0 - T$, increase exponentially with the rate γ , and terminate at the time t_0 of index modulation.

From Eq. (17) and the preceding discussion, we conclude that $U_c = U_s$ when $s_+(t)$ has the shape given in Eq. (18), $\gamma_e = \gamma$ (i.e., $\gamma_0 = 0$), and $\gamma T \rightarrow \infty$. In other words, one can transfer the total energy U_s of the incident pulse into the frequency-converted output if and only if the cavity has no

intrinsic loss and the pulse exciting it is semi-infinite and exponentially increasing with rate γ_e . Both of these requirements are physically unattainable, so one always obtains $U_c < U_s$.

The interpretation of Eq. (12) as an inner product also gives us a prescription for maximizing the converted energy $U_c = |a_c(t_0)|^2$ over a restricted set of pulse shapes $s_+(t)$ of equal energy U_s . This prescription consists of maximizing the projection of $s_+(t)$ along $h(t_0, t)$. For instance, consider the set of exponentially increasing pulses $s_+(t)$ of the form (18), but with γ replaced by a free parameter μ . It is straightforward (albeit tedious) to verify that indeed $\mu = \gamma$ results in the largest possible U_c , equal to the right-hand side of Eq. (17).

However, the usefulness of the preceding guideline is limited. This is because it only allows comparison between pulses of equal energy U_s and equal premodulation time T . Also, it might not be evident which pulse among a set of possible choices yields the largest projection along $h(t_0, t)$ and numerical evaluation of Eq. (12) may be required. Such a calculation is equivalent to solving the original problem of integrating Eq. (11); so no insight is gained from the prescription in this case. Nonetheless, as discussed in Sec. IV B, we show that this guideline is still useful to interpret the results of numerical optimization.

The requirements of no intrinsic loss and a semi-infinite, exponentially increasing $s_+(t)$ for 100% conversion efficiency can be understood via an argument based on the principles of energy conservation and reversibility. The argument is as follows. First, recall from Eq. (9) that the converted energy U_c is merely the energy in the cavity at the time of modulation, multiplied by a factor of γ_e/γ . However, for $U_c = U_s$ to occur, we need $\gamma_e = \gamma$, so in this ideal case, the converted energy and the energy in the resonator are identical. Thus, we only need to argue that when the cavity has zero intrinsic loss and it is excited by a semi-infinite, exponentially increasing pulse, all of the pulse's energy couples to the resonator.

To do so, consider energy dissipation in an ideal cavity with no intrinsic loss. Such an ideal cavity dissipates all of its energy by emitting a semi-infinite exponential pulse into the output port. After an infinite period of time, all of the energy stored in the cavity is released into the output port. If we reverse this process in time, it becomes the injection of a semi-infinite, exponentially increasing pulse into the cavity. From the time-reversal symmetry of Maxwell's equations, this reversed process is also a valid solution to them [31,34]. Thus, as required, we find that the energy in the exponentially increasing pulse must equal that deposited in the cavity, once the pulse is terminated.

Note that for this time-reversibility argument to agree with the purely mathematical Eq. (17), we required Eq. (5) to relate κ and γ_e . Therefore, Eq. (17) along with the same time-reversibility argument could be used conversely to establish Eq. (5). Indeed, such an argument follows the same physical reasoning, based on energy conservation and time reversibility, albeit slightly different mathematics, as the one originally employed by Haus [31] to derive Eq. (5).

IV. PULSED INPUT OF FIXED SHAPE

In this section we examine AFC when the input pulse has a fixed shape and finite energy. Our objective is to analyze the

effects of varying several relevant parameters such as relative values of the decay rates γ_0 and γ_e , the modulation time t_0 , and the input-pulse duration T_s .

Rather than working with the input signal $s_+(t)$ directly, it is more convenient to normalize $s_+(t)$ with respect to its duration T_s . Hence, we write $s_+(t)$ as

$$s_+(t) = \frac{1}{\sqrt{T_s}} \bar{s}_+ \left(\frac{t}{T_s} \right), \quad (19)$$

where $\bar{s}_+(\tau)$ is the normalized input-pulse profile subject to two conditions. The first condition is that it obeys the normalization

$$\int_{-\infty}^{\infty} d\tau |\bar{s}_+(\tau)|^2 = U_s. \quad (20)$$

Evidently, Eq. (14) then follows from Eqs. (19) and (20). The second condition is that $|\bar{s}_+(\tau)|^2$ is of the order of U_s only when $|\tau|$ is of the order of unity or lower. In other words, $|\bar{s}_+(\tau)|^2$ should be negligible, relative to U_s , for $|\tau| \gg 1$.

Substituting Eq. (19) into Eq. (11), we obtain

$$\frac{da_c}{d\tau} = -\bar{\gamma} a_c + \bar{\kappa} \bar{s}_+(\tau), \quad (21)$$

where $\tau = t_0/T_s$ is the normalized modulation time, $\bar{\gamma}$ the normalized decay rate, and $\bar{\kappa}$ the normalized coupling constant. These last two are defined as

$$\bar{\gamma} \equiv \gamma_0 T_s + \gamma_e T_s, \quad \bar{\kappa} \equiv \sqrt{2} \gamma_e T_s / \sqrt{\bar{\gamma}}. \quad (22)$$

Thus, for a fixed pulse shape $\bar{s}_+(\tau)$, the converted-energy amplitude a_c depends on three independent parameters: the normalized modulation time t_0/T_s , the normalized intrinsic decay rate $\gamma_0 T_s$, and the normalized external decay rate $\gamma_e T_s$.

To analyze the dependence of the converted-energy amplitude a_c on the modulation time, we consider input pulses of finite support such that $\bar{s}_+(\tau) = 0$ for $|\tau| > \tau_0$ and some τ_0 . For concreteness, we examine the case where the input pulse $\bar{s}_+(\tau)$ has the shape of a raised cosine, corresponding to

$$\bar{s}_+(\tau) = \sqrt{2U_s/3} [1 + \cos(2\pi\tau)] [H(\tau + \frac{1}{2}) - H(\tau - \frac{1}{2})]. \quad (23)$$

The raised-cosine shape in Eq. (23) is also known as the Hann (or Hanning) window function in the context of numerical Fourier analysis [35,36].

As desired, $\bar{s}_+(\tau)$ in Eq. (23) has a finite support: It is only nonzero for $|\tau| < \frac{1}{2}$. In addition, the Hann pulse has the desirable features of being continuous and having a continuous derivative for all real τ . Given Eq. (23) for $\bar{s}_+(\tau)$, both its full width at half maximum duration T_{FWHM} and root-mean-square duration T_{RMS} are straightforward to calculate. These are given by

$$T_{\text{FWHM}} = \frac{T_s \arccos(\sqrt{2} - 1)}{\pi} \approx 0.364 T_s, \quad (24)$$

$$T_{\text{RMS}} = \frac{T_s}{2} \sqrt{\frac{1}{3} - \frac{5}{2\pi^2}} \approx 0.141 T_s.$$

Equation (24) can be used to evaluate T_s in terms of experimentally measurable quantities.

In the remainder of this section, we study numerically the dependence of the energy efficiency η on the AFC's

timescales. Our objective is to determine how to choose these timescales to maximize η . To do this, we sweep the normalized timescales of the process and solve Eq. (21) for their corresponding values and for the raised-cosine input shape $\bar{s}_+(\tau)$ of Eq. (23). Note that the space spanned by the normalized parameters t_0/T_s , $\gamma_0 T_s$, and $\gamma_e T_s$ is three dimensional. Thus, we first perform partial parameter sweeps where only two of the three are swept while the other one is fixed. This allows us to visualize and understand the dependence of η on this reduced two-dimensional parameter space. Then we perform a global parameter sweep, where all three normalized parameters are swept simultaneously to identify optimum values for all parameters. To enable visualization and because we are mostly interested in optimization, we reduce the dimensionality of the parameter space in this global parameter sweep by considering only the optimum η over the normalized modulation time t_0/T_s .

A. Partial parameter sweeps

Having set Eq. (23) for $\bar{s}_+(\tau)$, we perform partial parameter sweeps of the solutions $a_c(\tau)$ to Eq. (11) and evaluate the corresponding energy efficiency $\eta = U_c/U_s$. The results are depicted in Fig. 2. Because we are interested in sweeping orders of magnitude of the parameter ratios rather than in examining the effect of small changes, we label them with logarithmic scales. Furthermore, because we are mostly interested in the maxima of $U_c [|a_c(\tau)|^2]$, we need only consider $\tau = t_0/T_s \in [-1/2, 1/2]$, as $\bar{s}_+(\tau)$ vanishes outside this range.

Figure 2(a) shows the results of our first parameter sweep. In it we set the resonator to critical coupling ($\gamma_e = \gamma_0$ [31]) and sweep t_0/T_s and $\gamma_0 T_s$. This figure can be interpreted as a visualization of η for different modulation times t_0 and pulse widths T_s , with fixed γ_0 and γ_e . The most prominent feature of Fig. 2(a) is the maximum in η occurring at $\gamma_0 T_s = 1.1768$ and $t_0/T_s = 0.2172$, where η reaches a value of 0.1987. This indicates that, for a critically coupled resonator, one should set the pulse duration T_s equal to $1.1768\gamma_0^{-1}$ and the modulation time t_0 to $0.2172T_s$ to achieve the maximum efficiency under critical coupling. This relatively low value suggests that, although critical coupling maximizes the resonator's energy for continuous-wave input [31], it is not the optimal choice to optimize the energy efficiency of AFC. We demonstrate this inference to be correct in Sec. IV B.

We highlight another feature of Fig. 2(a). This is that, for a given value of $\gamma_0 T_s$, the modulation time t_0 for maximum η decreases monotonically with increasing $\gamma_0 T_s$. To explain this feature, we note that $a_c(\tau)$ acts as the output of a first-order low-pass filter with a time constant $\bar{\gamma}^{-1}$. Moreover, because γ_e/γ_0 is fixed, the normalized decay $\bar{\gamma}$ scales linearly with $\gamma_0 T_s$, as a consequence of Eq. (22). If $\gamma_0 T_s \ll 1$, the shape of $a_c(\tau)$ resembles the integral of $\bar{s}_+(\tau)$ and its maximum lies close to $t_0 = T_s/2$. On the other hand, as $\gamma_0 T_s$ increases, $\bar{\gamma}^{-1}$ decreases and the shape $a_c(\tau)$ gradually resembles that of $\bar{s}_+(\tau)$, which has its maximum at $\tau = 0$.

In Fig. 2(b) we set $\gamma_0 T_s = 1$ while sweeping t_0/T_s and γ_e/γ_0 . This can be interpreted as fixing the intrinsic decay γ_0 and the pulse duration T_s while varying the modulation time t_0 and the extrinsic decay γ_e . Again, we find a choice of param-

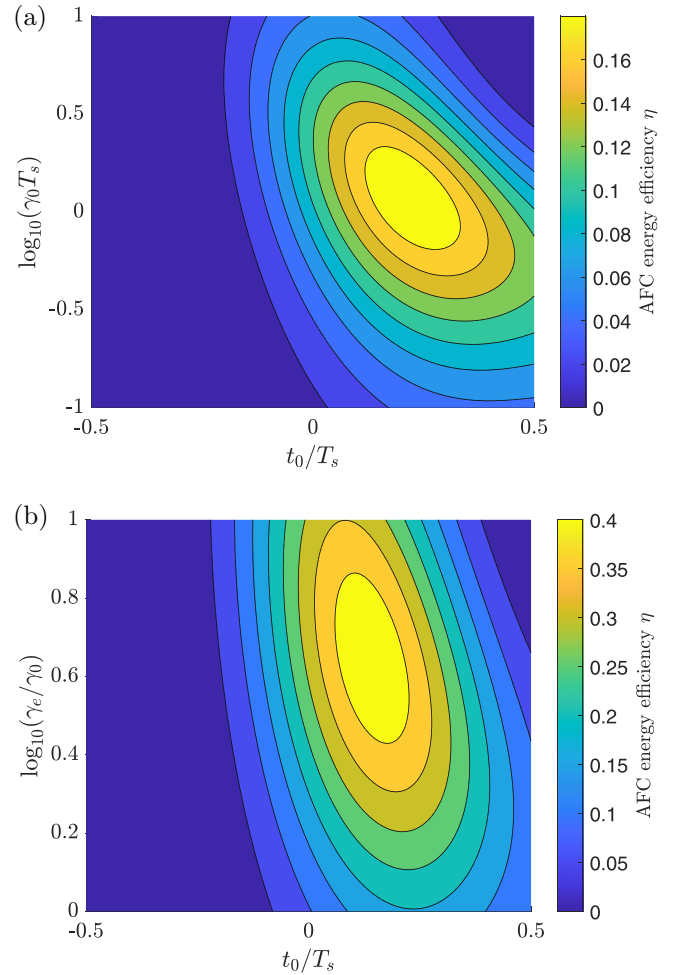


FIG. 2. Contour plots of the AFC energy efficiency η in the high-modulation limit for a Hann-shape input pulse. (a) AFC energy efficiency η in the case of critical coupling ($\gamma_e/\gamma_0 = 1$). (b) AFC energy efficiency η for a fixed value of the normalized pulse duration ($\gamma_0 T_s = 1$).

eters where the AFC efficiency peaks at a value $\eta = 0.4373$. The peak occurs at $\gamma_e = 4.4306\gamma_0$ and $t_0 = 0.1364T_s$. Thus, when the pulse duration T_s is of the order of γ_0^{-1} (twice the intrinsic photon lifetime), one should design the resonator to be slightly overcoupled ($\gamma_e > \gamma_0$) to achieve the maximum AFC efficiency. We observe that the modulation time t_0 for best efficiency decreases with increasing γ_e/γ_0 . Again, this can be understood by interpreting $a_c(\tau)$ as the output of a low-pass filter with the time constant $\bar{\gamma}^{-1}$.

B. Global parameter sweep

Now we perform a global parameter sweep, where we sweep the full parameter space by simultaneously varying all normalized parameters: the normalized modulation time t_0/T_s , the normalized pulse duration $\gamma_0 T_s$, and the normalized external decay γ_e/γ_0 . Once again, our objective is to identify the set of parameters which yield maximum AFC energy efficiency $\eta = U_c/U_s$. To allow visualization of the results, we collapse the dependence of η on t_0 by plotting only the maximum of η over t_0/T_s in the range $[-1/2, 1/2]$ for each pair of values for

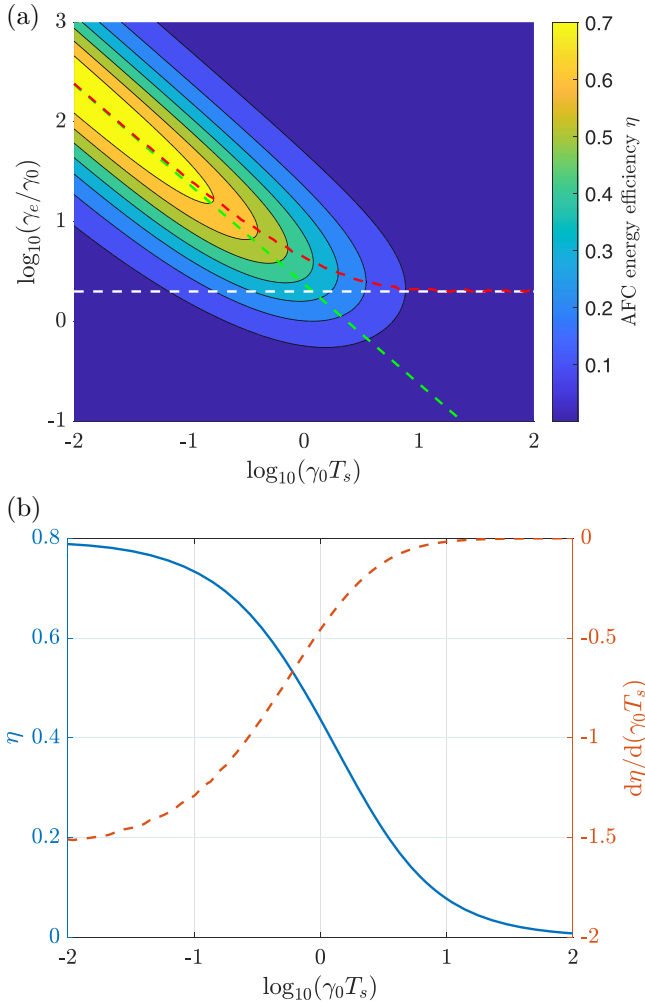


FIG. 3. Global parameter sweep of the AFC energy efficiency η over both the normalized pulse duration $\gamma_0 T_s$ and the normalized external decay γ_e/γ_0 , optimized over the modulation time t_0 , for an input Hann pulse in the high-modulation limit. (a) Contour plot of AFC energy efficiency η . The red dashed line depicts the locus of optimum γ_e for a given value of $\gamma_0 T_s$. The green dashed line indicates its asymptote for $\gamma_0 T_s \ll 1$; and the white dashed line, its asymptote for $\gamma_0 T_s \gg 1$. (b) Plot of the AFC energy efficiency η for a given normalized pulse duration $\gamma_0 T_s$ and maximized over the modulation time t_0 and external decay γ_e (blue solid line). Plot of the derivative of the AFC efficiency η (optimized with respect to t_0 and γ_e) as a function of $\gamma_0 T_s$ (orange dashed line).

$\gamma_0 T_s$ and γ_e/γ_0 . The result is shown in Fig. 3(a). Again, we use logarithmic scales $\gamma_0 T_s$ and γ_e/γ_0 . As is clear from Fig. 3(a), a necessary condition for maximizing η is to minimize $\gamma_0 T_s$. Moreover, as $\gamma_0 T_s \rightarrow 0$, the optimal γ_e that maximizes η for a given $\gamma_0 T_s$ converges to the asymptote

$$\gamma_e T_s = 2.3780, \quad \gamma_0 T_s \ll 1. \quad (25)$$

In Fig. 3(a), Eq. (25) corresponds to the straight line $\log_{10}(\gamma_e/\gamma_0) = \log_{10}(2.3780) - \log_{10}(\gamma_0 T_s)$ depicted graphically as a green dashed line. Equation (25) implies that, for $\gamma_0 T_s \ll 1$, a resonator needs to be significantly overcoupled to maximize the converted energy U_c , as also observed in Ref. [26]. To see this, note that if $\gamma_0 T_s \ll 1$, then $(\gamma_e/\gamma_0) \gg$

$\gamma_e T_s$ and $\gamma_e \gg \gamma_0$. This is also graphically evident from Fig. 3(a), where the line for Eq. (25) lies noticeably upward from the horizontal level $\log_{10}(\gamma_e/\gamma_0) = 0$.

To understand how Eq. (25) emerges, we consider the idealized case of a resonator with no intrinsic loss ($\gamma_0 = 0$). It follows from Eq. (22) that $\bar{\gamma} = \gamma_e T_s$ and $\bar{\kappa} = \sqrt{2\gamma_e T_s}$. As a result, η depends only on t_0/T_s and $\gamma_e T_s$. In this idealized case, we determine via numerical optimization that, for an input $\bar{s}_+(\tau)$ with a Hann pulse shape [Eq. (23)], η is maximized at $t_0/T_s = 0.2194$ and $\gamma_e T_s = 2.3780$ [matching Eq. (25)], attaining the value of $\eta = 0.7951$. From Sec. III we recall that maximization of η can be understood geometrically as the maximization of the magnitude of inner product in Eq. (12). As γ_0 increases from zero, it only slightly shifts the conditions and decreases the value of the maximum η , as long as it satisfies $\gamma_0 T_s \ll 1$ and $\gamma_0/\gamma_e \ll 1$. Specifically, an increasing, but still small, γ_0 slightly decreases the maximum attainable efficiency η and slightly shifts it towards larger values of γ_e .

Of course, the exact value of 2.3780 in Eq. (25) is particular to the Hann shape of the pulse in Eq. (23). Nonetheless, the Hann shape is generic in the sense that it represents a typical single-lobe pulse. Hence, an asymptote of the form

$$\gamma_e T_s = k, \quad k \sim 1, \quad \gamma_0 T_s \ll 1 \quad (26)$$

must exist for any single-lobe pulse shape. Furthermore, k can be determined by setting $\gamma_0 = 0$ and optimizing η over t_0/T_s and $\gamma_e T_s$, just as we did for the Hann pulse. As discussed in Sec. III, this value of k maximizes the magnitude of the inner product between the impulse response $h(t_0, t)$ and the input signal $s_+(t)$.

It follows from Eq. (26) that, when the energy efficiency η is maximized, the duration of output pulse is comparable to that of the input pulse. To see this, we recall from Eq. (11) that the frequency-shifted pulse is an exponentially decaying pulse with time constant of γ^{-1} . If Eq. (26) is satisfied, $\gamma^{-1} \approx \gamma_e^{-1} = T_s/k \sim T_s$. This result was first identified by Daniel *et al.* [26].

Although Eq. (26) maximizes the inner product, one cannot claim that it maximizes the projection of $s_+(t)$ over $h(t_0, t)$ or vice versa. This is because both $s_+(t)$ and $h(t_0, t)$ change as the ratios t_0/T_s , $\gamma_0 T_s$, and γ_e/γ_0 vary. Although $\bar{s}_+(\tau)$ does remain fixed, saying that Eq. (26) maximizes the projection of a renormalized $h(t_0, t)$ over $\bar{s}_+(\tau)$ is also misleading. This is because, as the parameter ratios are swept, the renormalized $h(t_0, t)$ changes its norm rather than just its “direction” in the Hilbert space of square-integrable functions.

As $\gamma_0 T_s$ approaches unity, the external coupling γ_e required for maximum η progressively increases away from Eq. (25). When $\gamma_0 T_s$ increases beyond unity, the γ_e required to maximize η is no longer well described by Eq. (25). In fact, the optimum γ_e converges to the asymptote

$$\gamma_e = 2\gamma_0, \quad \gamma_0 T_s \gg 1. \quad (27)$$

In Fig. 3(a), Eq. (27) corresponds to the horizontal line shown as a white dashed line. It implies that, even for $\gamma_0 T_s \gg 1$, the resonator needs to be overcoupled for efficient AFC, as observed in Sec. IV A.

To understand the origin of Eq. (27), we again examine Eq. (11) as a low-pass filter. When $\gamma_0 T_s \gg 1$, it follows from Eq. (22) that $\bar{\gamma}^{-1} \ll 1$, i.e. the response time $\bar{\gamma}^{-1}$ of $a_c(\tau)$

to $\bar{s}_+(\tau)$ becomes short. Consequently, the differential equation (11) approximates the algebraic relation

$$a_c(\tau) = \frac{\bar{k}\bar{s}_+(\tau)}{\bar{\gamma}}. \quad (28)$$

To maximize the converted energy $U_c = |a_c(\tau)|^2$ with respect to γ_e , the coefficient $\bar{k}\bar{\gamma}^{-1}$ should take its maximum value. Equation (27) then results from maximizing $\bar{k}\bar{\gamma}^{-1}$ with respect to γ_e . As implied by this argument, Eq. (27) does not depend on the shape of input pulses. This is in contrast to Eq. (26), where the precise value of k depends on the specific input pulse shape.

In Fig. 3(b) we consider a range of values of $\gamma_0 T_s$ and plot with a blue solid line the maximum AFC efficiency η attainable by tuning γ_e . Equivalently, these are the values of η along the red dashed line in Fig. 3(a), plotted as a function of their corresponding $\gamma_0 T_s$. The maximum possible η decreases monotonically with increasing $\gamma_0 T_s$. This verifies the intuitive notion that, for efficient AFC, one should have $\gamma_0 \ll T_s^{-1}$ and $\gamma_0 \ll \gamma_e$, i.e., the intrinsic decay should be small. Also, the efficiency is limited by the upper bound $\eta = 0.7951$. This value corresponds to $\gamma_0 = 0$ for a Hann pulse.

Figure 3(b) indicates that one must make $\gamma_0 T_s$ as small as possible to obtain the largest AFC efficiency. However, inspection of the plot for η in Fig. 3(b) by itself seemingly implies that decreasing $\gamma_0 T_s$ below unity results in diminishing returns. Specifically, decreasing $\gamma_0 T_s$ to $\gamma_0 T_s - \delta$ ($\delta > 0$) increases η to $\eta + \delta |d\eta/d(\gamma_0 T_s)|$, for small δ , and $|d\eta/d(\gamma_0 T_s)|$ appears to be maximized at $\gamma_0 T_s = 1$, according to the plot for η in Fig. 3(b). However, one must keep in mind that the horizontal axis in Fig. 3(b) employs a logarithmic scale. Thus, the local slope of the plot for η does not equal $d\eta/d(\gamma_0 T_s)$. For this reason, we numerically evaluate the derivative $d\eta/d(\gamma_0 T_s)$ and plot it as an orange dashed line in Fig. 3(b). This way, we realize that $|d\eta/d(\gamma_0 T_s)|$ increases monotonically with decreasing $\gamma_0 T_s$. Therefore, decreasing $\gamma_0 T_s$ to increase η actually never incurs diminishing returns, as one might have expected from inspection of only the blue solid curve in Fig. 3(b).

V. CONTINUOUS-WAVE INPUT

In this section we consider AFC with a continuous-wave (cw) input of fixed power P_0 . Without loss of generality, we suppose that this cw input is turned on at $t = 0$. We also assume that the rise time of $s_+(t)$ is negligible compared to the resonator's decay rates γ_0 and γ_e . In this case, we can write the input field $s_+(t)$ in Eq. (11) as

$$s_+(t) = \sqrt{P_0} H(t). \quad (29)$$

With this expression for $s_+(t)$, Eq. (11) can be solved for $a_c(t_0)$ in closed form. The solution corresponds to the step response of a first-order differential equation, well known from the theory of first-order electric circuits, i.e., RC and RL circuits [37]. From it we may immediately evaluate the converted energy U_c as

$$U_c = \frac{27}{4} \frac{\gamma_e^2 \gamma_0}{\gamma^3} U_c^{(\max)} [1 - \exp(-\gamma t_0)]^2, \quad (30)$$

where we have defined

$$U_c^{(\max)} = \frac{8}{27} \frac{P_0}{\gamma_0} \approx 0.296 \frac{P_0}{\gamma_0}. \quad (31)$$

When both P_0 and γ_0 are fixed, it follows from Eq. (30) that the maximum possible converted energy is indeed given by $U_c^{(\max)}$ in Eq. (31).

Because the cw input of Eq. (29) carries infinite energy U_s , we cannot normalize U_c with respect to U_s as in Sec. IV. Nonetheless, normalization of U_c is still useful, as it will allow us to perform a general parameter sweep, depending only on the ratios of the resonator and modulation timescales rather than their absolute magnitude. Hence, we take both the input power P_0 and the intrinsic decay rate γ_0 as fixed, normalize U_c with respect to the ratio $U_c^{(\max)}$ from Eq. (31), and examine the cw efficiency $\eta_{\text{cw}} \equiv U_c/U_c^{(\max)}$.

From Eq. (30) it is straightforward to verify that $\eta_{\text{cw}} < 1$. Furthermore, η_{cw} converges to unity when Eq. (27) is satisfied, with the pulse duration T_s replaced with the modulation time t_0 . Additionally, we note that, when Eq. (27) (with the substitution $T_s \rightarrow t_0$) is satisfied, the output pulse's duration γ^{-1} is necessarily much shorter than the modulation time because $\gamma^{-1} \sim \gamma_0^{-1} \ll t_0$.

Given Eq. (29) for $s_+(t)$, the cw efficiency η_{cw} depends only on the normalized modulation time $\gamma_0 t_0$ and the normalized decay rate γ_e/γ_0 . Therefore, we may visualize a global parameter sweep of η_{cw} with a simple contour plot. In Fig. 4(a) we present such a contour plot of η_{cw} as a function of $\gamma_0 t_0$ and γ_e/γ_0 . We only consider values $\gamma_0 t_0 > 0$, because γ_0 can only be positive and because $t_0 < 0$ results in $\eta_{\text{cw}} = 0$ in the high-modulation limit, as a consequence of Eq. (29).

Figure 4(a) corroborates that η_{cw} is maximized if and only if Eq. (27) is satisfied after the substitution $T_s \rightarrow t_0$. As in Fig. 3(a), we show with a red dashed line the curve corresponding to the locus of the values of γ_e that optimize η for a fixed $\gamma_0 t_0$ in Fig. 4(a). As identified above, for $\gamma_0 t_0 \gg 1$, this curve has Eq. (27) as an asymptote (with $T_s \rightarrow t_0$). This asymptote is shown as a green dashed line in Fig. 4(a). Similarly to Sec. IV, there exists a different asymptote for $\gamma_0 t_0 \ll 1$ given by the curve

$$\gamma_e t_0 = 1.2564, \quad \gamma_0 t_0 \ll 1. \quad (32)$$

To determine the value of 1.2564 in Eq. (32), we consider Eq. (30) for $\gamma_0 = 0$ and numerically optimize the resulting expression for U_c with respect to $\gamma_e t_0$. The straight line corresponding to Eq. (32) is shown as a white dashed line in Fig. 4(a).

As expected, Eq. (32) is of the form of Eq. (26), albeit with the pulse duration T_s replaced with the modulation time t_0 . Furthermore, we have already shown that the asymptote for $\gamma_0 t_0 \gg 1$ has the form of Eq. (27). Thus, both asymptotes in Fig. 4(a) are analogous to those in Fig. 3(a). Nonetheless, there is a clear difference between Fig. 3(a) for pulsed input and Fig. 4(a) for cw input. In Fig. 3(a) the optimum η is achieved when $\gamma_0 T_s \ll 1$, while in Fig. 4(a) the optimum η_{cw} is attained when $\gamma_0 t_0 \gg 1$.

We explain these similarities and differences between η and η_{cw} through the following argument. It is intuitively clear that the frequency-shifted energy U_c achieved with the cw input from Eq. (29) should be the same as that achieved

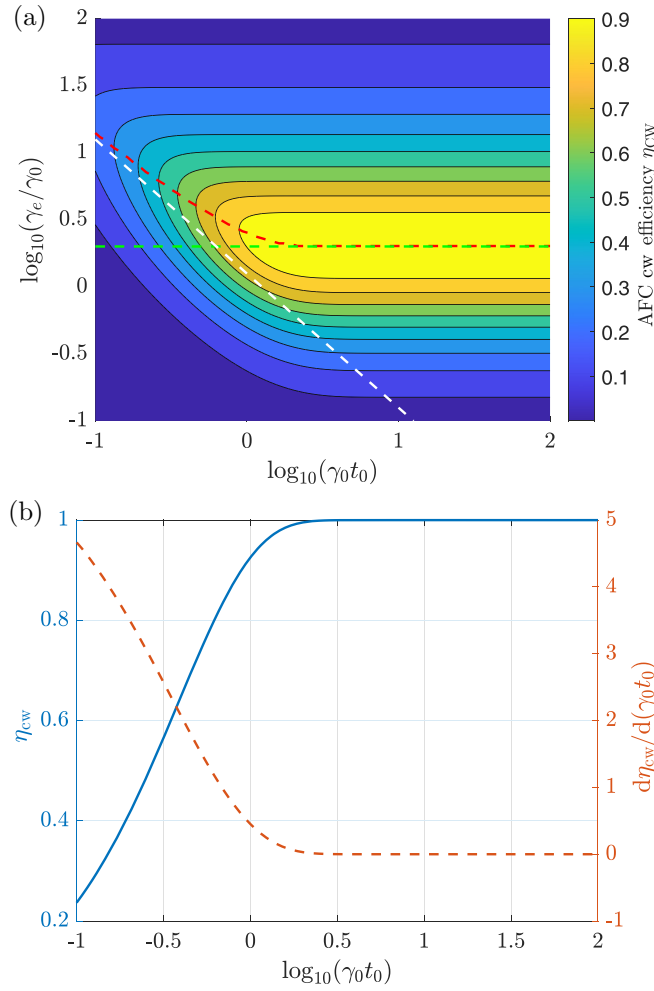


FIG. 4. Global parameter sweep for the optimization of the AFC energy efficiency η_{cw} for a cw input. (a) Contour plot of the AFC energy efficiency η_{cw} for a cw input. The red dashed line depicts the locus of optimum γ_e for a given value of $\gamma_0 t_0$; the green dashed line indicates its asymptote for $\gamma_0 t_0 \ll 1$; and the white dashed line shows its asymptote for $\gamma_0 t_0 \gg 1$. (b) Optimized η_{cw} as a function of $\gamma_0 t_0$ and maximized over γ_e (blue solid line) and its derivative as a function of $\gamma_0 t_0$ (orange dashed line).

with a rectangular input pulse that starts at $t = 0$ and ends at $t = t_0$ (duration $T_s = t_0$) and has total energy $U_s = P_0 t_0$. In evaluating η_{cw} , we normalize U_c with respect to $U_c^{(\max)}$, proportional to $P_0/\gamma_0 = U_s/(\gamma_0 t_0)$, rather than with respect to $U_s = P_0 t_0$. Therefore, η_{cw} in Fig. 4(a) can be understood as η for a square input pulse of duration $T_s = t_0$, albeit multiplied by a factor of $27\gamma_0 t_0/8$, as a consequence of normalization with respect to $U_c^{(\max)}$ in Eq. (31). The additional factor of $\gamma_0 t_0$ displaces the optimum normalized modulation time $\gamma_0 t_0$ from $\gamma_0 t_0 \ll 1$, as in Fig. 3(a), to $\gamma_0 t_0 \gg 1$, as in Fig. 4(a). The additional factor of $\gamma_0 t_0$ does not change the optimal γ_e for a given value of $\gamma_0 t_0$. Consequently, the curves of optimal γ_e for a pulsed square input and a cw input are the same. Recall that the asymptote in Eq. (26) is applicable for any single-lobe pulse, with only the value of k varying with the precise pulse shape, as argued in Sec. IV. Thus, the γ_e asymptotes for the Hann pulse are analogous to those for a square pulse. This

explains why the asymptotes in Fig. 4(a) resemble those in Fig. 3(a).

As in Sec. IV, we also examine how the maximum attainable η_{cw} varies with the normalized modulation time $\gamma_0 t_0$. This is equivalent to plotting the value of η_{cw} along the optimal γ_e curve of Fig. 4(a). The result is shown as the blue solid line in Fig. 4(b). Notice that, as $\gamma_0 t_0$ increases beyond unity, η_{cw} rapidly converges to 1. From Eq. (31) we verify that, since the maximum with respect to γ_e converges to $\gamma_e = 2\gamma_0$, the maximum η_{cw} for a fixed $\gamma_0 t_0$ converges to unity almost exponentially as $\gamma_0 t_0$ tends to infinity. In turn, this causes the derivative of η_{cw} (optimized with respect to γ_e) with respect to $\gamma_0 t_0$ to decay exponentially, as verified by inspection of the orange dashed line in Fig. 4(b). Therefore, increasing the modulation time $\gamma_0 t_0$ to increase η_{cw} incurs diminishing returns. To see this, we note as in Sec. IV B that increasing $\gamma_0 t_0$ to $\gamma_0 t_0 + \delta$ increases η_{cw} by $\delta \cdot d\eta_{cw}/d(\gamma_0 t_0)$ for small $\delta(\gamma_0 t_0)$. As $d\eta_{cw}/d(\gamma_0 t_0)$ decreases monotonically with $\gamma_0 t_0$, so does the gain in increasing $\gamma_0 t_0$. This situation contrasts with that for a pulsed input of Sec. IV B, where the increase in U_c due to a small decrease in $\gamma_0 T_s$ never results in diminishing returns.

VI. CONCLUSION

In this paper we presented a comprehensive theoretical analysis of the attainable energy efficiency of adiabatic frequency conversion. We invoked the Cauchy-Schwarz inequality and used it to obtain a theoretical bound for AFC efficiency, determine the optimal pulse shape to excite AFC, and analyze how the pulse shape determines AFC efficiency. Next we considered a fixed single-lobe input pulse shape and analyzed how the AFC efficiency depends on its various timescales. We showed that optimal AFC efficiency always requires resonator overcoupling, albeit with a degree varying with the input pulse duration. Then we examined the case where AFC is excited by a continuous-wave optical input. We again found that maximum output energy is achieved when the resonator is overcoupled. Additionally, we interpreted the conditions for optimal AFC under cw input in terms of the results of AFC for a pulsed input. Our results are useful to optimize any realization of AFC in an all-pass resonator. This will enable shifting work on AFC from proof-of-principle experiments to engineering for applications.

ACKNOWLEDGMENTS

The work was supported support by the National Science Foundation Grant No. ECCS-1807735. L.C.-H. acknowledges financial support from Mexico's National Council of Science and Technology.

APPENDIX: JUSTIFICATION FOR THE CONDITION IN EQ. (8)

Let $\tilde{a}_1(t)$ stand for the second term on the right-side of Eq. (7):

$$\tilde{a}_1(t) \equiv \int_{t_0}^t dt' \kappa s_+(t') \exp[(i\Delta_0 + \gamma)(t' - t_0)]. \quad (\text{A1})$$

In this Appendix we discuss the condition when $\tilde{a}_1(t)$ is negligible compared to $a(t_0)$, so $\tilde{a}(t)$ in Eq. (7) can be treated as a constant.

The integral in Eq. (A1) cannot be performed analytically for an arbitrary pulse shape $s_+(t)$. Because our goal is to find a rule of thumb rather than an exact formula, we choose a pulse shape suitable for analysis. Thus, for simplicity, we take $s_+(t)$ as a rectangular pulse. Then

$$s_+(t) = \sqrt{\frac{U_s}{T_s}} \left[H\left(t + \frac{T_s}{2}\right) - H\left(t - \frac{T_s}{2}\right) \right], \quad (\text{A2})$$

where U_s is the pulse's energy and T_s its duration.

Substituting Eqs. (5) and (A2) into Eq. (A1) and performing the integral, we obtain

$$|\tilde{a}_1(t)|^2 = \frac{4\gamma_e U_s}{(\Delta_0^2 + \gamma^2) T_s} \exp(\gamma t_m) \times [\cosh(\gamma t_m) - \cos(\Delta_0 t_m)], \quad (\text{A3})$$

where

$$t_m \equiv \min(T_s/2 - t_0, t - t_0). \quad (\text{A4})$$

As $a(t_0)$ in Eq. (7) is independent of Δ_0 , it follows from Eq. (A3) that for sufficiently large detuning Δ_0 , one must have $|\tilde{a}(t)|^2 \ll |a(t_0)|^2$. In this case, neglect of the second term on the right-hand side of Eq. (7) is justified. However, Eq. (A3) is a transcendental function of both Δ_0 and γ . Hence, it is useful to simplify it, even at the cost of generality. To do so, we consider the high-quality limit, in which $\gamma t_m \ll 1$. Then $\exp(\gamma t_m) \approx 1$ and $|\tilde{a}_1(t)|^2$ becomes bounded by

$$|\tilde{a}_1(t)|^2 \leq \frac{8\gamma_e U_s}{(\Delta_0^2 + \gamma^2) T_s}. \quad (\text{A5})$$

If we assume that the ring cavity has been excited efficiently, $|a(t_0)|^2 \sim U_s$. It follows that $|a(t_0)|^2 \ll |\tilde{a}_1(t)|^2$ if

$$8\gamma_e \ll (\Delta_0^2 + \gamma^2) T_s. \quad (\text{A6})$$

Usually in the case of AFC, we have $|\Delta_0| \gg \gamma$, so the post-modulation output can be resolved from the premodulation output. Using this feature, Eq. (A6) can be simplified to Eq. (8).

-
- [1] A. C. Turner-Foster, M. A. Foster, R. Salem, A. L. Gaeta, and M. Lipson, Frequency conversion over two-thirds of an octave in silicon nanowaveguides, *Opt. Express* **18**, 1904 (2010).
- [2] Q. Lin, J. Zhang, P. M. Fauchet, and G. P. Agrawal, Ultra-broadband parametric generation and wavelength conversion in silicon waveguides, *Opt. Express* **14**, 4786 (2006).
- [3] W. Mathlouthi, H. Rong, and M. Paniccia, Characterization of efficient wavelength conversion by four-wave mixing in sub-micron silicon waveguides, *Opt. Express* **16**, 16735 (2008).
- [4] S. Zlatanovic, J. S. Park, S. Moro, J. M. C. Boggio, I. B. Divliansky, N. Alic, S. Mookherjee, and S. Radic, Mid-infrared wavelength conversion in silicon waveguides using ultracompact telecom-band-derived pump source, *Nat. Photon.* **4**, 561 (2010).
- [5] B. E. A. Saleh and M. C. Teich, *Fundamentals of Photonics*, 3rd ed. (Wiley, Hoboken, 2019), pp. 1021–1065
- [6] A. Yariv and P. Yeh, *Photonics: Optical Electronics in Modern Communications*, 6th ed. (Oxford University Press, New York, 2007), pp. 358–380.
- [7] R. W. Boyd, *Nonlinear Optics*, 3rd ed. (Academic Press, Amsterdam, 2008), pp. 74–108.
- [8] M. F. Yanik and S. Fan, Dynamic photonic structures: Stopping, storage, and time reversal of light, *Stud. Appl. Math.* **115**, 233 (2005).
- [9] M. Notomi and S. Mitsugi, Wavelength conversion via dynamic refractive index tuning of a cavity, *Phys. Rev. A* **73**, 051803(R) (2006).
- [10] W. Pauli, *Statistical Mechanics* (Dover, Mineola, New York, 1973), pp. 85–87.
- [11] H. Goldstein, C. Poole, and J. Safko, *Classical Mechanics*, 3rd ed. (Addison Wesley, San Francisco, 2002), pp. 549–553.
- [12] S. F. Preble, Q. Xu, and M. Lipson, Changing the colour of light in a silicon resonator, *Nat. Photonics* **1**, 293 (2007).
- [13] S. Preble, L. Cao, A. Elshaari, A. Aboketaf, and D. Adams, Single photon adiabatic wavelength conversion, *Appl. Phys. Lett.* **101**, 171110 (2012).
- [14] T. Tanabe, M. Notomi, H. Taniyama, and E. Kuramochi, Dynamic Release of Trapped Light from an Ultrahigh- Q Nanocavity via Adiabatic Frequency Tuning, *Phys. Rev. Lett.* **102**, 043907 (2009).
- [15] R. Konoike, H. Nakagawa, M. Nakadai, T. Asano, Y. Tanaka, and S. Noda, On-demand transfer of trapped photons on a chip, *Sci. Adv.* **2**, e1501690 (2016).
- [16] T. Tanabe, E. Kuramochi, H. Taniyama, and M. Notomi, Electro-optic adiabatic wavelength shifting and Q switching demonstrated using a p-i-n integrated photonic crystal nanocavity, *Opt. Lett.* **35**, 3895 (2010).
- [17] N. Karl, P. P. Vabishchevich, M. R. Shcherbakov, S. Liu, M. B. Sinclair, G. Shvets, and I. Brener, Frequency conversion in a time-variant dielectric metasurface, *Nano Lett.* **20**, 7052 (2020).
- [18] W. Yoshiki, Y. Honda, M. Kobayashi, T. Tetsumoto, and T. Tanabe, Kerr-induced controllable adiabatic frequency conversion in an ultrahigh Q silica toroid microcavity, *Opt. Lett.* **41**, 5482 (2016).
- [19] Y. Minet, L. Reis, J. Szabados, C. S. Werner, H. Zappe, K. Buse, and I. Breunig, Pockels-effect-based adiabatic frequency conversion in ultrahigh- Q microresonators, *Opt. Express* **28**, 2939 (2020).
- [20] Y. Xiao, G. P. Agrawal, and D. N. Maywar, Spectral and temporal changes of optical pulses propagating through time-varying linear media, *Opt. Lett.* **36**, 505 (2011).
- [21] Y. Xiao, D. N. Maywar, and G. P. Agrawal, Optical pulse propagation in dynamic Fabry–Perot resonators, *J. Opt. Soc. Am. B* **28**, 1685 (2011).
- [22] B. A. Daniel, D. N. Maywar, and G. P. Agrawal, Dynamic mode theory of optical resonators undergoing refractive index changes, *J. Opt. Soc. Am. B* **28**, 2207 (2011).

- [23] M. Minkov, Y. Shi, and S. Fan, Exact solution to the steady-state dynamics of a periodically modulated resonator, *APL Photon.* **2**, 076101 (2017).
- [24] M. Minkov and S. Fan, Localization and time-reversal of light through dynamic modulation, *Phys. Rev. B* **97**, 060301(R) (2018).
- [25] M. R. Shcherbakov, P. Shafirin, and G. Shvets, Overcoming the efficiency-bandwidth tradeoff for optical harmonics generation using nonlinear time-variant resonators, *Phys. Rev. A* **100**, 063847 (2019).
- [26] B. A. Daniel, D. N. Maywar, and G. P. Agrawal, Efficient adiabatic wavelength conversion in Gires–Tournois resonators, *Opt. Lett.* **36**, 4155 (2011).
- [27] W. D. Sacher and J. K. Poon, Dynamics of microring resonator modulators, *Opt. Express* **16**, 15741 (2008).
- [28] P. Dong, S. F. Preble, J. T. Robinson, S. Manipatruni, and M. Lipson, Inducing Photonic Transitions between Discrete Modes in a Silicon Optical Microcavity, *Phys. Rev. Lett.* **100**, 033904 (2008).
- [29] J. Heebner, R. Grover, and T. Ibrahim, *Optical Microresonators: Theory, Fabrication, and Applications*, Springer Series in Optical Sciences Vol. 138 (Springer, New York, 2007), pp. 71–84.
- [30] V. Van, *Optical Microring Resonators: Theory, Techniques, and Applications* (CRC, Boca Raton, 2016), pp. 67–69.
- [31] H. A. Haus, *Waves and Fields in Optoelectronics* (Prentice Hall, Englewood Cliffs, 1984), pp. 200–207.
- [32] C. Manolatou, M. Khan, S. Fan, P. R. Villeneuve, H. Haus, and J. Joannopoulos, Coupling of modes analysis of resonant channel add-drop filters, *IEEE J. Quantum Electron.* **35**, 1322 (1999).
- [33] S. Hassani, *Mathematical Physics: A Modern Introduction to Its Foundations*, 2nd ed. (Springer International, Cham, 2013), p. 35.
- [34] V. S. Asadchy, M. S. Mirmoosa, A. Díaz-Rubio, S. Fan, and S. A. Tretyakov, Tutorial on electromagnetic nonreciprocity and its origins, *Proc. IEEE* **108**, 1684 (2020).
- [35] F. J. Harris, On the use of windows for harmonic analysis with the discrete Fourier transform, *Proc. IEEE* **66**, 51 (1978).
- [36] E. O. Brigham, *The Fast Fourier Transform and its Applications* (Prentice Hall, Englewood Cliffs, 1988), pp. 181–182.
- [37] C. K. Alexander and M. N. Sadiku, *Fundamentals of Electric Circuits*, 5th ed. (McGraw-Hill, New York, 2013), pp. 273–281.